In Situ Formation of Ag Nanoparticles in Spherical Polyacrylic Acid Brushes by UV Irradiation

Yan Lu,* Yu Mei, Marc Schrinner, Matthias Ballauff,* Michael W. Möller, and Josef Breu

Physikalische Chemie I, University of Bayreuth, 95440 Bayreuth, Germany, and Anorganische Chemie I, Universität Bayreuh, 95440 Bayreuth, Germany

Received: February 4, 2007; In Final Form: March 26, 2007

We reported on the in situ synthesis of silver nanoparticles onto polystyrene (PS) core−poly(acrylic acid) (PAA) polyelectrolyte brush particles. The synthesis of these composite particles proceeds through a photoemulsion polymerization in aqueous dispersion using the functional monomer silver acrylate. In this way the layer of the chains of poly(acrylic acid) on the surface and the Ag nanoparticles are formed at the same time. Dynamic light-scattering (DLS) measurement demonstrates the formation of polyelectrolyte brushes onto the PS core surface. TEM and cryo-TEM images show that well-dispersed Ag nanoparticles ($d = 3 \pm 1.2$ nm) are formed in situ on the surface of PS−PAA spherical polyelectrolyte brush particles. Moreover, wide-angle X-ray scattering indicates that Ag nanoparticles formed in the brushes are crystalline. The catalytic activity is investigated by monitoring the reduction of 4-nitrophenol by $NaBH_4$ in presence of these silver nanocomposite particles. The rate constant k_{app} of this reaction was found to be slightly smaller than the one of Pd or Pt nanoparticles immobilized on carrier particles of the same type. All data demonstrate that the present way of synthesis leads to extremely small Ag particles immobilized on a stable carrier.

1. Introduction

Nanoparticles consisting of noble metals have recently attracted much attention because such particles may exhibit unusual chemical and physical properties differing strongly from the properties of the bulk metal.[1] Thus, such nanoparticles have interesting perspectives in the applications as catalysts,[1−3] sensors,[4] and electronics. However, a capping agent is usually used in the synthesis of metal nanoparticles to both prevent the aggregation of the metal particles[5] and impart useful chemical behavior to the final nanoscale product. Until now, a great number of carrier systems have been developed for the immobilization of metal nanoparticles, such as dendrimers,[6−8] latex particles,[9−13] microgels,[14−23] or other polymers.[24−26] Silver nanoparticles are particularly interesting due to their roles as substrates in studies of surface-enhanced Raman scattering,[27] fluorescence,[15] and catalysis.[22] Oxidation[28] and aggregation[29] of Ag nanoparticles, however, prevented further applications up to now. For preparation of Ag particles, Ag ions are often reduced in the protective colloids by addition of reducing agents such as sodium borohydride.[30−31] In photochemical reduction, hydrated electrons or free organic radicals formed by γ-rays or UV light can also reduce metal ions to metals.[32−33]

Most of the synthetic procedures reported up to now lead to Ag-particles larger than 10 nm. Thus, Xu et al.[34] have prepared Ag nanoparticles by reduction of silver nitrate with 254 nm UV light in the presence of poly (N-vinylpyrrolidone) (PVP). The average particle size ranged from 15.2 to 22.4 nm. Sukhorukov et al.[35] have demonstrated the photoinduced synthesis of silver particles inside the restricted volume of polyelectrolyte capsules. Both small (∼5 nm) and large (∼8 nm) silver nanoparticles have been observed in the polyelectrolyte capsules. Moreover, ionizing radiation has been applied to synthesize colloidal metal nanoparticles, making use of organic radicals that are formed in the radiolysis of the solvent and added organic compounds.[36] Akashi et al.[37] have reported the in situ formation of Ag nanoparticles on the surface of poly(N-isopropylacrylamide)-coated polystyrene microspheres by using 2,2′-azobisisobutyronitrile (AIBN) for the generation of radicals. Here too rather large Ag nanoparticles with a diameter of 14 ± 4.7 nm are obtained.

The goal of the present work is the generation and stabilization of Ag nanoparticles with a size well below 10 nm. In the previous work, we have demonstrated that spherical polyelectrolyte brushes (SPB), that is, colloidal particles consisting of a solid polystyrene core and a dense surface layer of polyelectrolytes as, e.g., poly(acrylic acid)[38] can be used to immobilize metal ions that may be reduced to the respective nanoparticles.[39−41] While this method leads to well-defined Pt, Pd, Au, and Ru nanoparticles with narrow size distribution and size of a few nanometers only, it failed to produce defined silver nanoparticles. We obtained rather polydisperse particles with sizes well in excess of 10 nm. This is due to the strong tendency of Ag nanoparticles to aggregate.

In the present synthesis, silver nanoparticles and poly(acrylic acid) (PAA) chains are generated at the same time by photoemulsionpolymerization of the functional monomer silver acrylate. As shown in Figure 1, the synthesis of these composite particles can be carried out in three steps: In the first step, PS core particles are prepared by a conventional emulsion polymerization.[42−43] In a second step, these core particles will be covered by a thin layer of the photoinitiator HMEM which is a monomer at the same time. In the third step, radicals are generated on the surface of the particles by UV irradiation that starts the polymerization of the water-soluble functional monomer silver acrylate. This grafting-from strategy leads to a polyelectrolyte brush generated on the surface of the core particles.[42] At the same time, the Ag^+ counterions of the acrylic

* Corresponding authors. E-mails: yan.lu@uni-bayreuth.de; matthias.ballauff@uni-bayreuth.de.

10.1021/jp070973m CCC: $37.00
Published on Web 05/09/2007

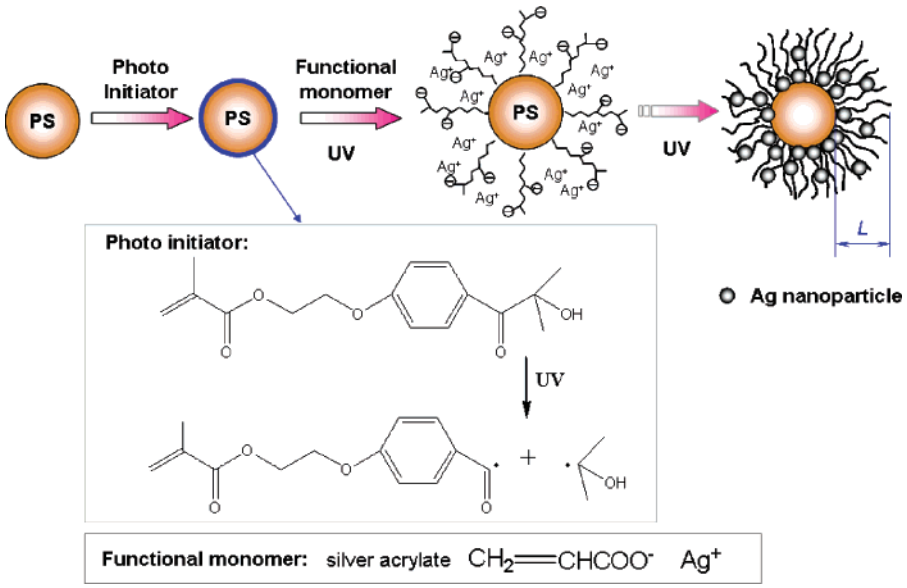

Figure 1. Schematic representation of the preparation of PS−PAA−Ag composite particles in situ. Poly(styrene) (PS) core particles are first prepared by a conventional emulsion polymerization. In a second step, the PS-cores are covered with a thin layer of photoinitiator HMEM. In the third step, the shell of polyelectrolyte brushes is formed by photoemulsion polymerization: shining light on the aqueous suspension of these particles generates radicals at their surface which initiate the radical polymerization of the functional monomer (silver acrylate) on the surface of the core particles. Concomitantly the silver anions embedded in the PAA brushes are reduced into Ag nanoparticles under UV irradiation.

acid are reduced to metallic Ag under UV irradiation. In this way the concentration of Ag^+ ions within the growing brush is kept low and the formation of large or undefined particles is prevented.

The paper is organized as follows: First we report on the synthesis and characterization of polystyrene (PS) core−poly(acrylic acid) (PAA) polyelectrolyte brush particles with silver nanoparticles. In a second part the resulting composite particles are analyzed in detail, most notably by cryogenic transmission electron microscopy (cryo-TEM).[44−46] Finally, the catalytic activity of silver nanocomposites is investigated using the reduction reaction of 4-nitrophenol by sodium borohydride.[2,40,47−48] Here we shall demonstrate that the Ag-composite particles present stable catalysts.

2. Experimental

2.1. Materials. Sodium dodecyl sulfate (SDS; Fluka), and potassium peroxodisulfate (KPS; Fluka) were used as received. Styrene (BASF) was purified by Al_2O_3 column and stored in the refrigerator. 2-[*p*-(2-Hydroxy-2-methylpropiophenone)]-ethyleneglycol methacrylate (HMEM) was used as the photoinitiator. The synthesis of this compound has been described previously.[42] Silver acrylate was purchased from ABCR and used as received.

2.2. Methods. Photoemulsion polymerization was done in a UV-reactor (Heraeus TQ 150 Z3, range of wavelengths 200−600 nm). Cryogenic transmission electron microscopy was done as outlined in ref 46.

Dynamic light scattering measurements were done using an ALV 4000 light scattering goniometer (Peters) at the angle of 90°. The UV spectra were measured by Lambda 25 spectrometer supplied by Perkin-Elmer. X-ray diffraction (XRD) measurement was performed at 25 °C on a Panalytical XPERT-PRO diffractometer in reflection mode using Cu Kα radiation. The silver content was determined by thermogravimetric analysis (TGA) using a Mettler Toledo STARe system. After drying in the vacuum overnight, the silver composites were heated to 800 °C with a heating rate of 10 °C/min under N_2. The theoretical specific surface area of silver particles was estimated from these TGA results, and the particle size was obtained from cryo-TEM. For this calculation, the density of bulk silver was used ($\rho = 10.5$ g/cm^3).

TABLE 1: Characterization of the PS−PAA−Ag Composite Particles

label	PS core[a] (g)	silver acrylate (g)	water (g)	R_{core}[b] (nm)	L[b] (nm)
PS−PAA−Ag	18.54	0.77	150	56.5	36.2

[a] Solid content for PS core dispersion is 8.09 wt. %. [b] R_{core} and L are measured by DLS at 25 °C.

2.3. Synthesis. PS core covered with a thin layer of photo initiator was prepared by conventional emulsion polymerization, which has been described in detail previously.[42] The PS−PAA−Ag composite particles were prepared by photoemulsion polymerization. Diluted PS core solution (1 wt %) was mixed with defined amount of functional monomer silver acrylate (30 mol-% with regard to the amount of styrene) under stirring. The whole reactor was degassed by repeated evacuation and subsequent addition of nitrogen at least 5 times. Photo polymerization was done by use of UV/vis radiation at room temperature for 90 min. Vigorous stirring ensured homogeneous conditions. To remove possible coagulum the latex was filtered over glass wool. Thereafter the silver nanocomposite particles were cleaned by dialysis against purified water (membrane: cellulose nitrate with 100 nm pore size supplied by Schleicher & Schuell).

All pertinent parameters, namely, the core radius R and the thickness L of the attached chains as determined by dynamic light scattering, are shown in Table 1.

2.4. Catalytic Reduction of 4-Nitrophenol. A 0.5 mL sample of sodium borohydride solution (60 mmol/l) was added to 2.5 mL of 4-nitrophenol solution (0.12 mmol/l) contained in a glass vessel. After that a given amount of the composite particles was added. Immediately after the addition of the composite-particles, UV spectra of the sample were taken every 30 s in the range of 250−550 nm. The rate constant of the reaction was determined by measuring the change in intensity of the peak at 400 nm with time.[47]

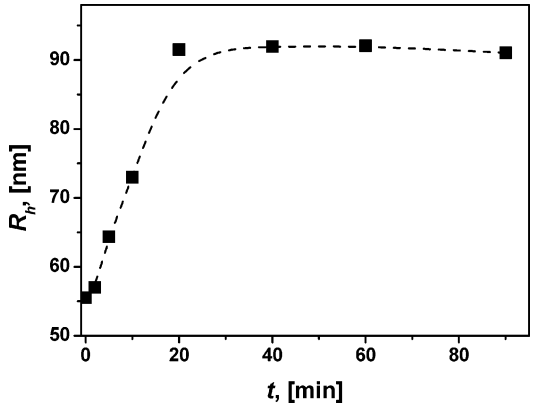

Figure 2. Increase of the particle size of PS−PAA−Ag with UV irradiation time as measured by DLS.

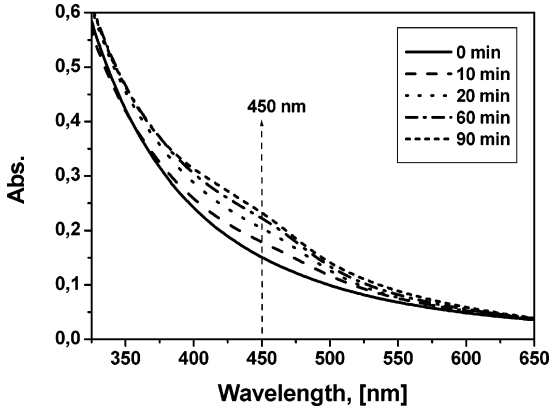

Figure 3. Formation of Ag nanoparticles in the PS−PAA brushes with UV irradiation time measured by UV−vis spectroscopy.

3. Results and Discussion

3.1. In Situ Formation of Ag Nanocomposite Particles. The synthesis of PS core particles by emulsion polymerization, and polyelectrolyte brushes by photopolymerization has been reported recently by us.[42−43] More recently, we have reported that spherical polyelectrolyte brush particles can work as carrier system for the generation and immobilization of metal nanoparticles.[39−41] In these polyelectrolyte brush systems, metal ions can be confined as counterions within the brush layer. Subsequent reduction of the metal salt within the "nanoreactors" thus defined leads to gold, platinum or palladium nanoparticles. In the present study, silver nanoparticles are in situ formed on the surface of PS−PAA brush particles by choosing functional monomer silver acrylate as the water-soluble monomer for the photopolymerization (see Figure 1). In principle, the radicals formed by photolysis of the HMEM groups on the PS core surface will start the radical polymerization of the shell. Under UV irradiation acrylic monomer will form the polyelectrolyte brushes affixed onto the PS core surface. The new feature is that the Ag^+ counterions of the acrylic acid will be reduced at the same time by the radicals to yield metallic Ag. In this way the local concentration of Ag^+-ions will be kept low which is expected to reduce the size of the Ag-nanoparticles.

The formation of the brush was confirmed by the increase in particle size measured by dynamic light scattering as shown in Figure 2. Since the radius of the PS core particles is known, DLS leads directly the thickness L of the brush layer. From Table 1, $L = 36.2$ nm has been obtained for the PS−PAA brush particles when 30 mol-% monomer was used for photopolymerization. This indicates that the PS cores are covered by a homogeneous shell of PAA brush during the photopolymerization. Moreover, the appearance of yellow color in the obtained brush solution demonstrates that Ag^+ ions have been reduced to metallic Ag by the radicals in the system.

It is known that nanometer-sized silver particles exhibit strong surface plasmon absorption at about 400−450 nm, the position of which is dependent on the factors such as particle size, shape, and dielectric properties of the surrounding media.[49] Figure 3 shows the changes in the UV−vis absorption spectra of PS−PAA−Ag composites with time. Before UV irradiation, no absorption can be observed in the range of 375 to 650 nm in the UV/vis spectra. Just after 10 min of irradiation, the composite solution becomes lightly yellow and the spectrum displays a broad absorption band at 450 nm, which corresponds to the formation of Ag clusters. The color of the solution then turns to darker yellow at longer irradiation times as more and more metallic silver particles are formed. However, the absorption at 450 nm only increases, no shift of the wavelength of absorption was found with time. This indicates that only the number of the Ag nanoparticles increases but there is no aggregation of these particles to larger clusters. It is worth noting that the colloid stability of silver composite particles is quite stable. Neither sedimentation nor the shift of the maximal of the surface plasmon absorption band was observed for the purified samples after storing for months. This fact points clearly to the effective protection of silver nanoparticles against aggregation or release from the polyelectrolyte brushes.

Figure 4a presents the typical TEM image for PS−PAA−Ag composite particles. From the TEM image, it can be seen clearly that practically monodisperse Ag nanoparticles have been generated in situ by UV irradiation, which are homogeneously embedded into PS−PAA brushes. This is also accord with the results from TGA measurement that 3.4 wt % Ag has been embedded. The analysis of the TEM image indicates that silver nanoparticles are relatively narrow dispersed with the diameter of 3 ± 1.2 nm. The particle size distribution histogram of Ag nanoparticles evaluated from TEM image is shown in Figure 4c.

Figure 4b displays the cryo-TEM image for silver nanocomposites. It is shown that small black silver nanoparticles are all located on the spherical PS−PAA brush particle surface, which is accord with the morphology of the cationic polyelectrolyte brush-metal composite particles obtained previously.[40−41,50] No metal particles can be observed outside of the brush particles. This indicates that the in situ formed Ag nanoparticles can be effectively immobilized by the spherical polyelectrolyte brushes. Moreover, no aggregates are visible in Figure 4b while Figure 4a reveals some larger objects on the surface of the core particles. However, since the TEM pictures in Figure 4a refer to the dry state while Figure 4b to the particles in situ, that is, in the aqueous phase, the larger particles visible in Figure 4a may well be a drying artifact.

The crystallinity of the PS−PAA−Ag composite particles was analyzed using X-ray diffraction (XRD) (Figure 5). A typical XRD pattern of as-prepared silver composites shows broad Bragg reflections at $2\theta = 38.2°$, 44.3°, 64.5°, 77.4°, and 81.5°, which are corresponding to the (111), (200), (220), (311), and (222) reflections of *fcc* (face centered cubic) structure of metallic silver, respectively.[33,51] This demonstrates that silver nanoparticles formed in the brushes are crystalline. These data are in excellent agreement with data in the Powder Diffraction File (PDF-No.: 00-004-0783). No diffraction peaks corresponding to silver oxide are observed, which confirms that only metallic Ag is formed in situ by UV irradiation.

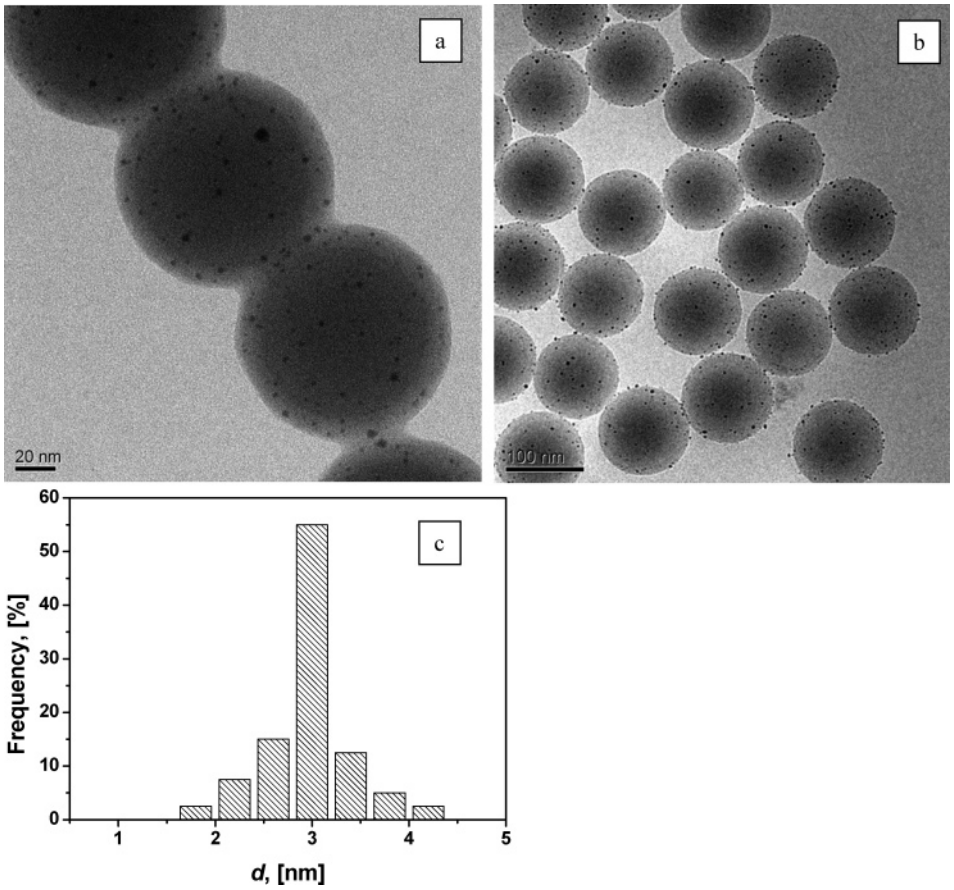

Figure 4. TEM (a) and cryo-TEM (b) images for the PS−PAA−Ag composite particles, and (c) the particle size distribution histogram of Ag particles evaluated from the TEM image (a).

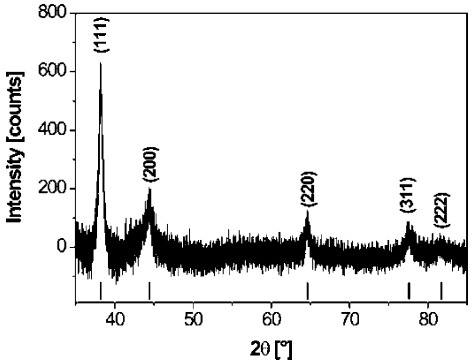

Figure 5. XRD pattern of the PS−PAA−Ag composite particles. Ticks indicate reference peaks for *fcc*-silver (PDF-No. 00-004-0783).

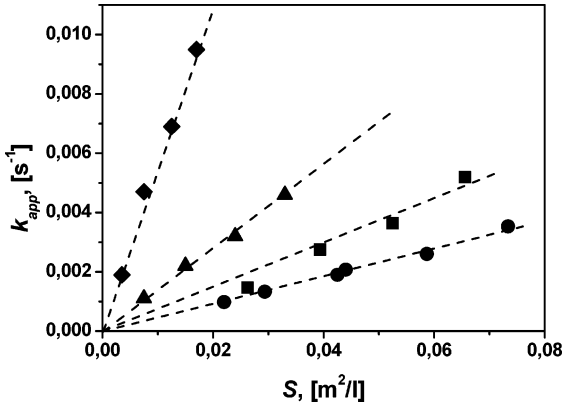

Figure 6. Rate constant k_{app} as function of the surface area S of metal nanoparticles normalized to the unit volume of the system. Squares, PS−PAA−Ag composite particles (this work); circles, microgel−Ag composite particles [ref 23]; triangles, microgel−Pd composite particles [ref 41]; diamonds, SPB−Pt composite particles [ref 40]. $T = 20$ °C; [4-nitrophenol] = 0.1 mmol/L, [$NaBH_4$] = 10 mmol/L.

All results obtained here indicate clearly that the present process involves a controlled nucleation and a limitation in growth of Ag nanoparticles which also do not aggregate. As shown by Figure 3, only the number of Ag nanoparticles increases during synthesis, not their size. Apparently, heterogeneous nucleation in the PAA-brushes is fostered while the subsequent growth of supercritical particles is limited by the small Ag^+ concentration during the synthesis of the particles and the restricted diffusion of Ag^+ in the polyelectrolyte environment. Hence, the new way of generating the Ag nanoparticles in spherical polyelectrolyte brushes restricts the particle sizes to the early stages of growth of supercritical nuclei. Additionally, any subsequent reaction as aggregation or coalescence is prevented.

3.2. Catalytic Activity. In order to investigate the catalytic activity of in situ formed silver nanocomposite particles, the reduction of 4-nitrophenol by an excess of $NaBH_4$ has been chosen as the model reaction. In this way the results can directly be compared to the data supplied by literature.[23,47−48,50,52] The kinetics of this reaction can be monitored by UV/vis spectroscopy. After addition of silver nanocomposite particles the peak at 400 nm which is due to the 4-nitrophenate ions decreases gradually with time and a new peak appears at 290 nm. This peak is due to the product 4-aminophenol.[53−54] The concentration of sodium borohydride was adjusted to largely exceed the concentration of 4-nitrophenol. Therefore in this case a first-order rate kinetics with regard to the 4-nitrophenol concentra-

TABLE 2: Catalytic Activity of the Metal Nanoparticles for the Reduction Reaction of 4-Nitrophenol

sample	carrier system	metal	D^a (nm)	$k_1{}^b$ ($s^{-1}\,m^{-2}L$)
PS−PAA−Ag	anionic polyelectrolyte brush (SPB); this work	Ag	3 ± 1.2	7.81×10^{-2}
ref 23	PS−NIPA core−shell microgel	Ag	8.5 ± 1.5	5.02×10^{-2}
ref 48	Highly branched polymer brush	Ag	7.5 ± 2	7.27×10^{-2}
ref 47	PVA polymer	Ag	~25	3.78×10^{-7}
ref 52	PVA/PS−PEGMA composite hydrogel	Ag	35 ± 5	7.80×10^{-5}
ref 52	PVA hydrogel	Ag	45 ± 5	7.31×10^{-5}
ref 40	cationic polyelectrolyte brush (SPB)	Pt	2.1 ± 0.4	0.55
ref 41	cationic polyelectrolyte brush (SPB)	Pd	2.4 ± 0.5	1.5
ref 50	cationic polyelectrolyte brush (SPB)	Au	1.25 ± 0.25	0.31
ref 41	PS−NIPA core−shell microgel	Pd	3.8 ± 0.6	1.01×10^{-1}

[a] *D*: diameter of the metal nanoparticles measured from cryo-TEM images. [b] k_1: rate constant normalized to the surface of the particles in the system (eq 1).

tions could be used to evaluate the catalytic rate. Furthermore, the apparent rate constant k_{app} will certainly be proportional to the total surface S of the metal nanoparticles present in the system:[23,40]

$$-\frac{dc_t}{dt} = k_{app}c_t = k_1 S c_t \quad (1)$$

where c_t is concentration of 4-nitrophenol at time t, and k_1 is the rate constant normalized to S, the surface area of Ag nanoparticles normalized to the unit volume of the system.

A linear relation between $\ln(c_t/c_0)$ versus time t has been obtained in all cases (see Supporting Information). The apparent rate constant k_{app} can be directly obtained from the curve of $\ln(c_t/c_0)$ versus time t by linear fit. Figure 6 shows the values of the apparent rate constant k_{app} as a function of theoretical specific surface area of PS−PAA−Ag nanoparticles together with systems containing other metal nanoparticles. For the calculation of the rate constants k_{app} normalized to the surface area in unit volume of the system, the bulk density of silver ($\rho = 10.5 \times 10^3$ kg/m^3) has been used.

As shown in Figure 6, a strictly linear relation between k_{app} and the surface of the metal nanoparticles can be observed. This has been found for all other systems shown in Figure 6 as well and ensures a direct comparison of all data. Figure 6 demonstrates that Pt and Pd nanoparticles exhibit higher catalytic activity than Ag nanoparticles. Table 2 summarizes the rate constants of all systems shown in Figure 6 together with other reported systems normalized to the surface area of the nanoparticles per unit volume. First of all, Table 2 indicates that comparison with other silver composite particles, in situ formed silver nanoparticles exhibit quite high catalytic activity, which is due to the smaller particle size and free diffusion of the reactant in the latex particles. Second, comparison with other metal composite particles (Au, Pt, Pd) prepared by similar carrier system, the catalyst activity is Pd > Pt > Au > Ag, which may be due to the different kinetic barriers of the reaction for different metal particles. This is also accord with the results reported by Pal et al.[55] A more detailed investigation of this point is under way by now.

It is interesting to note that both for Ag and Pd composite particles, the catalytic activity of metal nanoparticles immobilized in the polyelectrolyte brush system is higher than that of the microgel system. This can be explained by the diffusion speed of reactant molecules to metal nanoparticles encapsulated in both carrier systems. For the microgel system, the metal nanoparticles are immobilized in the cross-linked PNIIPA shell, thus reactant molecules need a longer time to reach catalytic active center. While in the case of polyelectrolyte system that has an open structure, reactant molecules can diffuse in latex particles and reach metal nanoparticles more quickly. This demonstrates that spherical polyelectrolyte brush particles can work as stable carrier systems for metal nanoparticles used in catalysis.

Conclusion

Well-dispersed Ag nanoparticles are formed in situ on the surface of polystyrene (PS) core-poly(acrylic acid) (PAA) polyelectrolyte brush particles by photoemulsion polymerization of Ag−acrylate. Dynamic light scattering (DLS) measurement demonstrates the formation of polyelectrolyte brushes onto the PS core surface. Cryo-TEM image shows that monodisperse Ag nanoparticles ($d = 3 \pm 1.2$ nm) are immobilized on the surface of PS−PAA spherical polyelectrolyte brush particles. Moreover, Ag nanoparticles in situ formed in the brushes are crystalline. The PS−PAA−Ag composite particles show high catalytic activity for the reduction reaction of 4-nitrophenol in the presence of sodium borohydride. Hence, the novel process reported here allows us to use silver nanoparticles in catalysis in the way demonstrated recently for platinum or palladium.

Acknowledgment. The authors thank the Deutsche Forschungsgemeinschaft, SFB 481, Bayreuth, and Schwerpunktprogramm "Hydrogele" (SPP1259/1), the BASF-AG, and Fonds der Chemischen Industrie for financial support.

Supporting Information Available: Influence of the concentration of the Ag-composite particles on the reduction of 4-nitrophenol. This material is available free of charge via the Internet at http://pubs.acs.org.

References and Notes

(1) Burda, C.; Chen, X.; Narayanan, R.; El-Sayed, M. A. *Chem. Rev.* **2005**, *105*, 1025.
(2) Praharaj, S.; Nath, S.; Ghosh, S.; Kundu, S.; Pal, T. *Langmuir* **2004**, *20*, 9889.
(3) Campbell, C. T.; Parker, S. C.; Starr, D. E. *Science* **2002**, *298*, 811.
(4) Frederix, F.; Friedt, J.; Choi, K.; Laureyn, W.; Campitelli, A.; Mondelaers, D.; Maes, G.; Borghs, G. *Anal. Chem.* **2003**, *75*, 6894.
(5) Ahmadi, T. S.; Wang, Z. L.; Green, T. C.; Henglein, A.; El-Sayed, M. A. *Science* **1996**, *272*, 1924.
(6) Scott, R. W. J.; Wilson, O. M.; Crooks, R. M. *J. Phys. Chem. B* **2005**, *109*, 692.
(7) Esumi, K.; Isono, R.; Yoshimura, T. *Langmuir* **2004**, *20*, 237.
(8) Liu, Z. L.; Wang, X. D.; Wu, H. Y.; Li, C. X. *J. Colloid Interface Sci.* **2005**, *287*, 604.
(9) Chen, C. W.; Serizawa, T.; Akashi, M. *Langmuir* **1999**, *15*, 7998.
(10) Sun, Q.; Deng, Y. *Langmuir* **2005**, *21*, 5812.
(11) Kim, J. W.; Lee, J. E.; Ryu, J. H.; Lee, J. S.; Kim, S. J.; Han, S. H.; Chang, I. S.; Kang, H. H.; Suh, K. D. *J. Polym. Sci., Part A: Polym. Chem.* **2004**, *42*, 2551.
(12) Mohammed, H. S.; Shipp, D. A. *Macromol. Rapid Commun.* **2006**, *27*, 1774.
(13) Carotenuto, G. *Appl. Organometal. Chem.* **2001**, *15*, 344.

(14) Zhang, J.; Xu, S.; Kumacheva, E. *J. Am. Chem. Soc.* **2004**, *126*, 7908.
(15) Zhang, J.; Xu, S.; Kumacheva, E. *Adv. Mater.* **2005**, *17*, 2336.
(16) Vincent, T.; Guibal, E. *Langmuir* **2003**, *19*, 8475.
(17) Biffis, A.; Orlandi, N.; Corain, B. *Adv. Mater.* **2003**, *15*, 1551.
(18) Biffis, A.; Sperotto, E. *Langmuir* **2003**, *19*, 9548.
(19) Xu, H.; Xu, J.; Zhu, Z.; Liu, H.; Liu, S. *Macromolecules* **2006**, *39*, 8451.
(20) Pich, A.; Hain, J.; Lu, Y.; Boyko, V.; Prots, Y.; Adler, H. J. *Macromolecules* **2005**, *38*, 6610.
(21) Pich, A.; Karak, A.; Lu, Y.; Boyko, V.; Adler, H. J. *Macromol. Rapid Commun.* **2006**, *27*, 344.
(22) Lu, Y.; Mei, Y.; Drechsler, M.; Ballauff, M. *Angew. Chem., Int. Ed. Engl.* **2006**, *45*, 813.
(23) Lu, Y.; Mei, Y.; Drechsler, M.; Ballauff, M. *J. Phys. Chem. B* **2006**, *110*, 3930.
(24) Suzuki, D.; Kawaguchi, H. *Langmuir* **2005**, *21*, 8175.
(25) Mbhele, Z. H.; Salemane, M. G.; Van Sittert, C. G. C. E.; Nedeljkovic, J. M.; Djolovic, V.; Luyt, A. S. *Chem. Mater.* **2003**, *15*, 5019.
(26) Doty, R. C.; Tshikhudo, T. R.; Brust, M.; Fernig, D. G. *Chem. Mater.* **2005**, *17*, 4630.
(27) Pileth, W. J. *J. Phys. Chem.* **1982**, *86*, 3461.
(28) Henglein, A. *Chem. Mater.* **1998**, *10*, 444.
(29) Mandal, S.; Gole, A.; Lala, N.; Gonnade, R.; Ganvir, V.; Sastry, M. *Langmuir* **2001**, *17*, 6262.
(30) Sau, T. K.; Pal, A.; Pal, T. *J. Phys. Chem. B* **2001**, *105*, 9266.
(31) Narayanan, R.; El-Sayed, M. A. *J. Phys. Chem. B* **2004**, *108*, 8572.
(32) Esumi, K.; Suzuki, A.; Aihara, N.; Usui, K.; Torigoe, K. *Langmuir* **1998**, *14*, 3157.
(33) Cheng, D.; Zhou, X.; Xia, H.; Chan, H. S. O. *Chem. Mater.* **2005**, *17*, 3578.
(34) Huang, H. H.; Ni, X. P.; Loy, G. L.; Chew, C. H.; Tan, K. L.; Loh, F. C.; Deng, J. F.; Xu, G. Q. *Langmuir* **1996**, *12*, 909.
(35) Shchukin, D. G.; Radtchenko, I.; Sukhorukov, G. B. *Chem. Phys. Chem.* **2003**, *4*, 1101.
(36) Henglein, A.; Ershov, B. C.; Malow, M. *J. Phys. Chem.* **1995**, *99*, 14129.
(37) Chen, C. W.; Chen, M. Q.; Serizawa, T.; Akashi, M. *Adv. Mater.* **1998**, *10*, 1122.
(38) Rühe, J.; Ballauff, M.; Biesalski, M.; Dziezok, P.; Gröh, F.; Johannsmann, D. *Adv. Polym. Sci.* **2004**, *165*, 79.
(39) Sharma, G.; Ballauff, M. *Macromol. Rapid Commun.* **2004**, *25*, 547.
(40) Mei, Y.; Sharma, G.; Lu, Y.; Drechsler, M.; Ballauff, M.; Irrgang, T.; Kempe, R. *Langmuir* **2005**, *21*, 12229.
(41) Mei, Y.; Lu, Y.; Polzer, F.; Ballauff, M.; Drechsler, M. *Chem. Mater.* **2007**, *19*, 1062.
(42) Guo, X.; Weiss, A.; Ballauff, M. *Macromolecules* **1999**, *32*, 6043.
(43) Guo, X.; Ballauff, M. *Langmuir* **2000**, *16*, 8719.
(44) Nizri, G.; Magdassi, S.; Schmidt, J.; Talmon, Y. *Langmuir* **2004**, *20*, 4380.
(45) Li, Z.; Kesselman, E.; Talmon, Y.; Hillmyer, M. A.; Lodge, T. P. *Science* **2004**, *306*, 98.
(46) Wittemann, A.; Drechsler, M.; Talmon, Y.; Ballauff, M. *J. Am. Chem. Soc.* **2005**, *127*, 9688.
(47) Pradhan, N.; Pal, A.; Pal, T. *Colloids Surf., A* **2002**, *196*, 247.
(48) Lu, Y.; Mei, Y.; Walker, R.; Ballauff, M.; Drechsler, M. *Polymer* **2006**, *47*, 4985.
(49) Mulvaney, P. *Langmuir* **1996**, *12*, 788.
(50) Schrinner, M.; Polzer, F.; Mei, Y.; Lu, Y.; Haupt, B.; Goeldel, A.; Drechsler, M.; Preussner, J.; Glatzel, U.; Ballauff, M. *Macromol. Chem. Phys.*, submitted for publication.
(51) Jiang, G. H.; Wang, L.; Chen, T.; Yu, H. J.; Wang, J. *J. Mater. Sci.* **2005**, *40*, 1681.
(52) Lu, Y.; Spyra, P.; Mei, Y.; Ballauff, M.; Pich, A. *Macromol. Chem. Phys.* **2007**, *208*, 254.
(53) Antipov, A. A.; Sukhorukov, G. B.; Fedutik, Y. A.; Hartmann, J.; Giersig, M.; Moehwald, H. *Langmuir* **2002**, *18*, 6687.
(54) Ghosh, S. K.; Mandal, M.; Kundu, S.; Nath, S.; Pal, T. *Appl. Catal., A* **2004**, *268*, 61.
(55) Pradhan, N.; Pal, A.; Pal, T. *Langmuir* **2001**, *17*, 1800.